

# OpenSlot: Mixed Open-set Recognition with Object-centric Learning

Xu Yin, Fei Pan, Guoyuan An, Yuchi Huo, Zixuan Xie, Sung-Eui Yoon

**Abstract**—Existing open-set recognition (OSR) studies typically assume that each image contains only one class label, and the unknown test set (negative) has a disjoint label space from the known test set (positive), a scenario termed full-label shift. This paper introduces the mixed OSR problem, where test images contain multiple class semantics, with known and unknown classes co-occurring in negatives, leading to a more challenging super-label shift. Addressing the mixed OSR requires classification models to accurately distinguish different class semantics within images and measure their “knowness”. In this study, we propose the OpenSlot framework, built upon object-centric learning. OpenSlot utilizes slot features to represent diverse class semantics and produce class predictions. Through our proposed anti-noise-slot (ANS) technique, we mitigate the impact of noise (invalid and background) slots during classification training, effectively addressing the semantic misalignment between class predictions and the ground truth. We conduct extensive experiments with OpenSlot on mixed & conventional OSR benchmarks. Without elaborate designs, OpenSlot not only exceeds existing OSR studies in detecting super-label shifts across single & multi-label mixed OSR tasks but also achieves state-of-the-art performance on conventional benchmarks. Remarkably, our method can localize class objects without using bounding boxes during training. The competitive performance in open-set object detection demonstrates OpenSlot’s ability to explicitly explain label shifts and benefits in computational efficiency and generalization.

**Index Terms**—Mixed Open-set Recognition, Object-centric Learning, Open-set Object Detection.

## I. INTRODUCTION

Open-set recognition (OSR) assumes the test samples come from open space [3], [4], [10], aiming to reject those having unknown classes (*negative*) and maintaining models’ classification performance on known classes (*positive*). This scenario is vital to ensure the safety of machine learning systems, and has been widely applied in various fields, e.g., fault detection [15] and medical diagnosis [14], where “unknownness” may happen anywhere and anytime.

Currently, OSR is categorized as a generalized Out-of-distribution (OOD) detection task [41], where the unknown classes are regarded as a label shift relative to the known classes. A standard OSR pipeline is to train a multi-class classification model on the known training images and compute a score [27], [36] to measure the test sample’s “knowness” and decide whether to reject or accept.

The present OSR framework (Fig. 1, (a)) builds upon an ideal condition: every test image is single-label. It leads to biased assumptions: the negative image only contains unknown classes, yielding two completely different label spaces of positive and negative images (termed a full-label shift).

Nevertheless, real images are often multi-labeled, with mixed known and unknown class objects. In this study, we

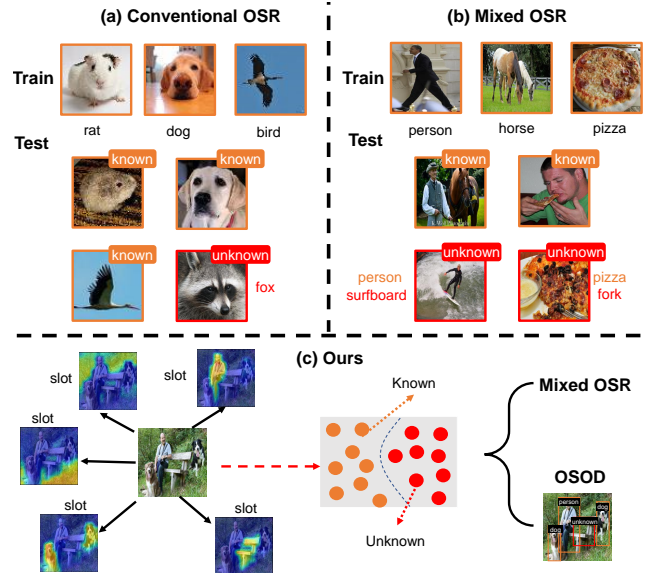


Fig. 1: (a) Conventional OSR assumes test samples only contain one class semantic (single-label) and regards images from new classes as unknown. (b) We propose the mixed OSR problem, which tests on images with multiple classes. The negative samples contain known and unknown classes and require the classifier to accurately detect the occurrence of unknown classes. (3) Existing methods can easily ignore the unknown class due to the existence of the known content. To address this issue, we propose using slots for semantic representation and producing independent class predictions. Thus, we learn a clear known/unknown decision boundary. Besides, our method can localize the unknown class and realize open-set object detection (OSOD).

formulate a **mixed OSR** problem (Fig. 1, (b)) that considers test samples with multiple class semantics, which is more commonly seen in real life. In each negative image, the known and unknown classes occur jointly. In this setting, the class set of negative images is the super-set of positives. Therefore, we define the mixed OSR as the super-label shift.

Discriminating images containing different class types requires the classification model to distinguish all object semantics clearly. Existing methods usually aggregate class semantics and compute an overall score for OSR evaluation. This approach has a risk: the classifier can be misled by known classes in the images, ignore the unknown content, and thus make an incorrect decision. Resorting to object detection and semantic segmentation approaches can be a good choice for accurately identifying the unknown class object. However, using the pixel and bounding box labels for training would inevitably increase the computation cost and

have generalization concerns [11], [30].

Recently, object-centric learning [28] has achieved promising results in multi-object representation [5], [33]. The slot features are bound with different object semantics and carry various object property information, e.g., size and location, thus facilitating different downstream vision tasks [17], [43].

Motivated by these advances [33], [35], we present a novel OpenSlot framework, propose learning slot features to represent the different class semantics, and implement image classification to handle the mixed OSR. To isolate the invalid and suspicious background slots during classification, we specifically propose a simple yet effective anti-noise-slot (ANS) technique to address the semantic misalignment problem of the class prediction. Combined with out-of-distribution (OOD) detection scoring metrics, we measure the “knownness” of the object semantic that each slot corresponds to, and achieve significant improvements on various OSR benchmarks. Additionally, our method could explicitly detect unknown objects without using bounding boxes for training, achieving competitive results in open-set object detection.

In summary, our contributions are three-fold:

- We introduce the mixed OSR task, which requires detecting unknown class objects in images with known content.
- We develop an OpenSlot framework based on object-centric learning. With the proposed anti-noise-slot (ANS) technique, we exclude the invalid and background semantics captured by slots from classification and address the semantic misalignment of class prediction.
- Extensive experiments show OpenSlot exceeds prevalent OSR studies considerably on various mixed & conventional benchmarks. Further, our method achieves meaningful open-set object detection results and demonstrates benefits in computational cost and generalization.

## II. RELATED WORK

**Open-set recognition (OSR).** OSR targets detecting the semantic novelties (i.e., label shift) in the test samples. Prevalent studies [2], [29] usually assume that negative images have a completely different label space from positives, termed the full-label shift. Popular OSR methods include prototype learning [16] and generative techniques [29]. For example, CSSR [16] models each known class prototype with an independent auto-encoder manifold to better measure class belongingness. DIAS [29] uses GAN to simulate unknown samples, thus improving the classification training. Despite advancing results in detecting the full-label shift in the conventional single-label classification, the complex super-label shift that occurs in images with multiple class types has never been explored. In this work, we present the mixed OSR problem and propose a novel object-centric learning framework to overcome the displayed semantic misalignment problem.

**Object-centric learning (OCL).** OCL [31], [33], [35] represents image semantics with a fixed number of feature vectors named slots. Each slot binds with an object or denotes an independent meaningful semantic and captures its object properties. Compared with CNN/ViT-based models, empirical studies [5], [31] demonstrated that slot-based representation is generalizable and robust against different distribution shifts. With

these intriguing properties, OCL has been applied to various vision tasks, such as image generation [17], [35], tracking [43]. Recently, Dinosaur [33] introduced self-supervised feature reconstruction as the objective function and first achieved real-world object-centric representations without using priors.

Motivated by these advances, we introduce OCL to handle the mixed OSR. With the proposed ANS technique, we represent diverse image semantics with slots and adapt slot-based predictions for image classification. Combined with existing out-of-distribution (OOD) detection metrics [27], [38], we conduct the slot-based OSR.

**Open-set object detection (OSOD).** OSOD targets localizing unknown objects during inference and shares a similar problem definition as out-of-distribution object detection [8], [39]. There are two main directions in this field: one line aims to break the limit on the category number and recognize more class objects beyond the closed set. For example, Grounding DINO [26] combines with the power of language models [39] and proposes a cross-modality fusion solution to fuse text and image features at different phases, thus detecting arbitrary class objects. The other line concentrates on unknown detection for safety purposes. For instance, VOS [8] generates virtual outliers in training and uses them to estimate a decision boundary between the known and unknown class objects. However, most existing methods [7], [26] are built upon well-trained object detectors, requiring expensive bounding box labels for training. In this study, we target unknown object detection and extend our classification approach to OSOD, achieving competitive results while offering various benefits.

## III. MIXED OPEN-SET RECOGNITION

In this section, we introduce the mixed OSR and illustrate its difference from the conventional OSR problem setting.

OSR [10], [41] needs to train a multi-class classifier to 1) classify test samples that fall into “known known classes (KKC)” and 2) detect test samples containing “unknown unknown classes (UUC)”. KKC indicates the known training categories (denoted with  $\mathcal{K}$ ), and UUCs represent the novel category group (denoted with  $\mathcal{A}$ ) that only occurs during inference. The occurrence of new categories at the test time is considered a label shift regarding the set of  $\mathcal{K}$ .

Let  $\mathcal{D}_{train}$  and  $\mathcal{D}_{test}^k$  ( $k$ : known) be the known training and test set (labeled *positive*), and their label space is  $\mathcal{K}$  consistently. We denote the unknown test set with  $\mathcal{D}_{test}^u$  ( $u$ : unknown) that contains UUCs (labeled *negative*), and express its label space with  $\mathcal{Y}$ . At the test time, we require the classifiers to accurately recognize negatives when processing samples from  $\mathcal{D}_{test}^k$  and  $\mathcal{D}_{test}^u$ .

The conventional OSR problem assumes that each image has a single label and considers no KKC exist in  $\mathcal{D}_{test}^u$ , i.e.,  $\mathcal{Y} = \mathcal{A}$ . This implies that each negative image  $\mathbf{x}_i \in \mathcal{D}_{test}^u$  only has UUC and  $\mathcal{D}_{test}^u$  and  $\mathcal{D}_{test}^k$  have entirely disjoint label spaces, i.e.,  $\mathcal{Y} \cap \mathcal{K} = \emptyset$ ; we refer to this setting as **full-label shift**. While this formulation simplifies the OSR problem by making certain assumptions about the content composition of  $\mathbf{x}_i$ , it may not fully capture the complexities of real-world scenarios where label shifts can occur in more diverse forms.

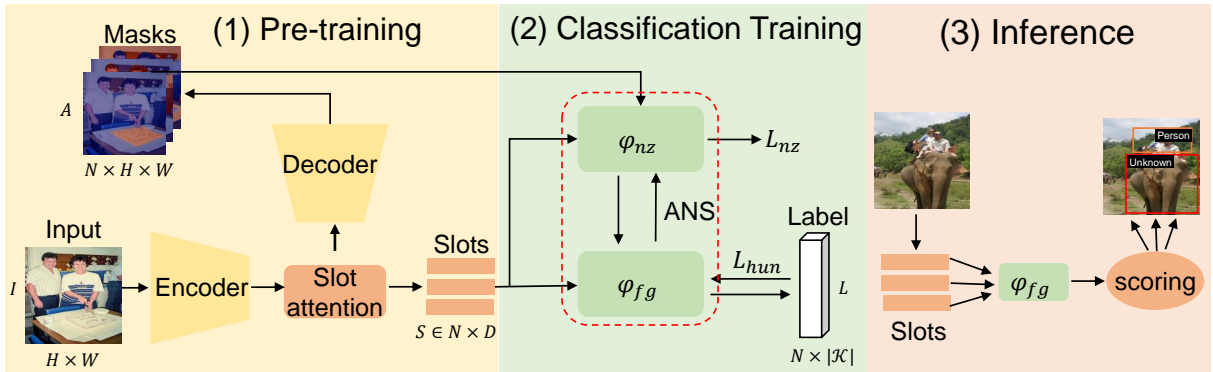


Fig. 2: OpenSlot overview. In (1), we pre-train Dinosaur [33] (following the encoder-decoder design, the encoder can be either ResNet or Transformer architecture) on the known training images, using slots  $S$  to learn class semantics. Next (2), we add two classifiers, the noise classifier  $\varphi_{nz}$  and the main classifier  $\varphi_{fg}$ , trained with  $L_{nz}$  (Eq. 2) and  $L_{hun}$  (Eq. 4) respectively, to identify the noise (invalid and background) slots and implement semantic classification with the proposed ANS technique (Fig. 3). During inference (3), we score slot-based class predictions to address the mixed OSR.

**Mixed OSR:** In an unpredictable open space, we consider the mixed scenario, where the negative image  $\mathbf{x}_i$  contains different category types, a common occurrence in real-world settings.

In this setting, we use  $y_i$  to denote  $\mathbf{x}_i$ 's class label set and get  $y_i \cap \mathcal{K} \neq \emptyset$  and  $y_i \cap \mathcal{A} \neq \emptyset$ . Following this setup, we get  $\mathcal{Y} = \mathcal{A} \cup \mathcal{K}$  and see that the distribution shift happens in the superset of  $\mathcal{K}$  (termed **super-label shift**).

Handling this mixed problem necessitates OSR models to recognize all class objects within the negative sample  $\mathbf{x}_i$  and group them as known or unknown. Besides, detecting the super-label shift in images with multiple class semantics is crucial for extending OSR to multi-label scenarios; a larger label space implies more mixture scenarios, with distribution shifts potentially manifesting anywhere. This capability directly benefits real-world applications, such as autonomous driving, species discovery, medical imaging analysis [14], and defect detection [15] in manufacturing processes.

Intuitively, classifying an image with multiple semantics can be significantly influenced by the known class objects. One potential solution is to use pre-trained dense predictors, e.g., object detector [32] and segmentation methods [19], to exhaustively classify each object proposal and pixel for precise identification. However, this approach needs more label information in training and can be computationally expensive (compared in Sec. V-E). Besides, their OSR performance relies heavily on dense predictors, which suffer from domain shifts [30]. These challenges motivate us to develop a classification model to obtain generalizable representations of diverse semantics within images and learn clear decision boundaries among different category groups to perceive label shifts.

#### IV. METHOD

In this part, we first introduce object-centric learning (OCL) and clarify the motivations. Next, we propose an OpenSlot framework to handle the mixed open-set recognition (OSR).

##### A. Preliminary: Object-centric learning

The goal of OCL [18], [28] is to represent the visual input with a set of object features (termed slots), with which to obtain the compositional representation of the input to

facilitate downstream vision tasks [17], [43]. In training, slot are randomly initialized and refined by an iterative attention module [28], to capture an independent object semantic.

OCL commonly adopts the autoencoder design and uses input reconstruction as the objective function. Recently, Dinosaur [33] proposes reconstructing the self-supervised features, e.g., DINO [1], during training and scales OCL to natural images, achieving the first success in the unsupervised setting. When combining the Transformer decoder [35], Dinosaur represents objects belonging to the same class with one slot, showing the potential of slot-based image classification. **Motivations.** We propose utilizing slot features to perform multi-class semantic classification and address the mixed OSR.

Firstly, each slot represents a particular object semantic and produces an independent class prediction. When evaluating the “knowness” of a negative image, the slot representing unknown classes (UUCs) contributes a significant score value difference compared to known classes. In contrast, existing methods [37], [38] typically aggregate all semantics to obtain an overall class prediction. Consequently, the resulting OSR score can be largely influenced by the known classes (KCCs) present in the input (Section V-D compares our slot-based method with existing studies regarding OSR scoring).

Secondly, slots inherently carry spatial location information [28], [33] of the represented objects, enabling our work to localize unknown object semantics and display the super-label shift of the test sample explicitly. Remarkably, relying solely on class labels during training, our method is capable of performing open-set object detection (OSOD) and achieves competitive performances (see Sec. V-E).

##### B. OpenSlot

The full framework has three stages. Firstly, we conduct unsupervised pretraining to endow slots with semantic representation ability. Next, we implement the slot-based image classification. With the proposed anti-noise-slot (ANS) technique, we exclude noisy slot features from the classification process, allowing the classifier to focus on true class objects. During inference, we score slot predictions using Out-of-distribution (OOD) detection metrics to make OSR decisions.

**Unsupervised pre-training:** To begin with, we train Dinosaur [33] on the KKC training set  $\mathcal{D}_{train}$ .

For each  $I \in \mathcal{D}_{train}$  ( $I \in \mathbb{R}^{H \times W \times 3}$ ), we get a set of slots  $S = \{S_1, \dots, S_N\}$  and their attention masks  $A$  (Fig. 2 (1)):

$$\{S, A\} = \text{Dinosaur}(I), \quad (1)$$

note that  $S \in \mathbb{R}^{N \times D}$  and  $A \in \mathbb{R}^{N \times H \times W}$ ,  $D$  denotes the slot dimension. Following the setup in [33], all slots  $S_i \in S$  are first initialized and randomly sampled from a common distribution. These slots then compete to reconstruct the self-supervised DINO [1] features.

In this work, we mainly adopt the ViT [6] encoder and Transformer decoder [34], [35], and  $S$  tends to capture category-level semantics. Other designs are compared and discussed in Sec. V. Note that regardless of the encoder/decoder architecture, pixels in  $A$  denote the importance of the corresponding slot in reconstructing the patch features.

**Slot-based image classification:** In addition to semantic representation, slots  $S$  capture useful object property information that can benefit downstream prediction tasks [5], [28]. In this section, we leverage the object properties encoded in the slots to perform image classification.

Following the practices in [5], [28], [31], we first pad (with null) the ground-truth categorical vector to make it of the same size as the slot set  $S$ . Next, we get its one-hot representation  $\mathbf{L} \in \mathbb{R}^{N \times |\mathcal{C}|}$  ( $|\mathcal{C}|$  denotes the number of training classes).

A naive solution (we termed Pure Slot) for obtaining class predictions is employing a shared classifier across all slots to generate per-slot predictions. The sum of cross-entropy losses from these predictions is then used as the assignment cost for Hungarian matching [28]. This matching result implements a set-to-set mapping between slot predictions and class labels and is then used to compute the training loss.

However, the number of slots  $N$  is fixed during training; OCL learns invalid slots [28] when  $N$  is larger than that of practical semantics. Meanwhile, the slots that represent background information also increase the difficulty of matching. These two issues would cause a severe misalignment problem, i.e., the final classification decision does not actually represent the class object content of the image. To address these limitations (shown and ablated in Sec. V-C), we propose the anti-noise-slot (ANS) technique to mitigate the effects of noise (invalid and background) slots on image classification.

Firstly, we add an MLP classifier  $\varphi_{fg}$  (shared across slots) after the slot-attention encoder to implement class prediction and matching. To isolate the invalid slots, we consider the attention masks  $A$  (shown in Fig. 3) a vital cue that provides rich information for the separation. We use a threshold  $\alpha$  to determine the semantic region of  $A$ , and assume that to denote a valid object semantic (foreground/background unknown), the slot’s attention mask should have over two consecutive pixels (corresponding to patch features) over  $\alpha$ . In this step, we use a mask  $M_{inv} \in \mathbb{R}^{N \times 1}$  for the invalid slot separation.

Next, we add another shared MLP classifier  $\varphi_{nz}$  (shown in Fig. 2 (2)) to accurately discriminate noise slots. In each classification training step, we get the mask of null slots (not matched with any object class in the label  $\mathbf{L}$ ), and take a union

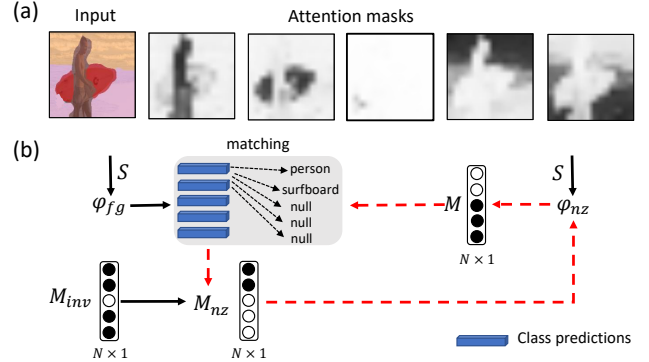


Fig. 3: Anti-noise-slot (ANS). After pre-training, we learned slot  $S$  to (a) represent the input’s diverse semantics (shown in different colors) and get their attention masks (each slot has an attention mask). (b) In each step of the classification training, we: 1) first merge the null slot mask with the invalid slot mask  $M_{inv}$  to get the pseudo label  $M_{nz}$ ; (2) use  $M_{nz}$  to train the noise classifier  $\varphi_{nz}$ ; (3) get the high-confidence prediction  $M$  from  $\varphi_{nz}$  to calibrate (Eq. 4) the assignment cost of Hungarian matching, enabling  $\varphi_{fg}$  to focus on true class semantics.

with  $M_{inv}$ . This way, we build up the pseudo label  $M_{nz} \in \mathbb{R}^N$  and train  $\varphi_{nz} \in$  with the noise loss  $L_{nz}$ :

$$L_{nz} = \text{BCE}(\varphi_{nz}(S), M_{nz}), \quad (2)$$

where BCE is a Binary Cross Entropy loss. Note that the unmatched slots contain suspicious background semantics; we combine them with the invalid slots, and train the noise classifier  $\varphi_{nz}$  for accurate discrimination.

To mitigate noise slots’ effect on the foreground semantic matching, we get the high-confidence (over a threshold  $\beta$ , after Min-max normalization) predictions  $M \in \mathbb{R}^{N \times 1}$  from  $\varphi_{nz}$ :

$$M = \mathbf{1}[(\varphi_{nz}(S) > \beta)]. \quad (3)$$

Let  $L_{set} = \text{CE}(\varphi_{fg}(S), \mathbf{L})$  be the pairwise loss between the slot predictions  $\varphi_{fg}(S)$  and the label set  $\mathbf{L}$ , where CE is cross-entropy loss. With the noise mask information from  $M$ , we recalibrate the assignment cost of Hungarian matching as:

$$L_{hun} = (1 - M) \cdot L_{set} + \lambda M \cdot L_{set}, \quad (4)$$

$\lambda$  is a large scalar to make noise slots of extremely high assignment costs in the matching process, thus reducing their probability of being matched with the true classes in  $\mathbf{L}$ .

As shown in Fig. 3, masks  $M$  and  $M_{nz}$  are constructed based on the prediction of  $\varphi_{nz}$  and  $\varphi_{fg}$ , respectively. These masks are then used as supervision ( $M_{nz} \rightarrow \varphi_{nz}$ ) and recalibration ( $M \rightarrow L_{hun}$ ) of each other’s classifiers. This self-supervised technique encourages the main classifier  $\varphi_{fg}$  to output low-value logits for noise slots and increases the magnitude difference between noise slots and foreground slots, which represent true class semantics. Meanwhile, the invalid slot mask  $M_{inv}$  is constructed heuristically (with the threshold  $\alpha$ ) and stabilizes the early training of slot classification.

**Framework Overview.** As illustrated in Fig. 2, we firstly pre-train Dinosaur [33] on  $\mathcal{D}_{train}$  (the training set of known classes) to obtain the representative slot features. Next, we frozen the Dinosaur part and added two classifiers,  $\varphi_{nz}$

and  $\varphi_{fg}$ , following the encoder. After excluding the noise slots from the semantic matching, we implement the image classification. The overall loss is expressed as follows:

$$L = L_{hun} + L_{nz}. \quad (5)$$

Note that the encoder and decoder part is frozen during the classification training, and all computation overhead comes from the classifiers  $\varphi_{nz}$  and  $\varphi_{fg}$ .

**Inference.** To get the classification result in the closed set, we use the max-logit slot in single-label experiments and the maximum class-wise logit across all slots in multi-label cases.

For OSR tasks, we score slot predictions with common OOD detection functions [13], [23], [24], [27]. The score measures the label shift degree of the content that each slot corresponds to. Lastly, we sum all scores as the decision score.

OpenSlot can also localize objects to realize open-set object detection, thus explicitly displaying the label shift. We treat attention masks as object proposals and use the over-threshold regions to produce the bounding box results. Based on corresponding OSR scores, we distinguish close-set and open-set objects and assign the known classes and “unknown” labels.

## V. EVALUATION

### A. Experiment setup

In this section, we first outline the experimental setup for different OSR tasks and show OpenSlot’s effectiveness. We also conduct extensive ablation studies to validate the impact of our design and compare OpenSlot with existing studies.

#### Benchmarks & Experiments.

- **Mixed OSR:** We mainly test on Pascal VOC (VOC) [9] and MS COCO (COCO) [25] datasets. To depict OSR tasks, we use the values before and after the slash to denote the number of known known classes (KKCs) and unknown unknown classes (UUCs), respectively. Our benchmarks have two types: single-label and multi-label, indicating whether the classification model is trained on **single-label** or **multi-label** known training sets.

For single-label benchmarks, we select images with only one class label from two datasets for training, constructing VOC-6/14 and COCO-20/60, respectively. In the multi-label cases, where each training image has more than one labeled class, we build four benchmarks: VOC-COCO (20/60) and COCO-20/60, 40/40, 60/20. VOC-COCO takes VOC classes as KKCs and the non-overlapping 60 COCO classes as UUCs. For the other three benchmarks, we randomly select 20, 40, and 60 COCO classes as KKCs, respectively, and use the remaining COCO classes as UUCs.

After the classification training, we evaluate models on test images with multiple class semantics. Throughout all experiments, we construct two types of unknown test sets  $D_{test}^u$ : the homogeneous ( $\mathcal{H}$ , where each image contains only UUCs) and the mixed ( $\mathcal{M}$ , where UUCs are mixed with KKCs). This comprehensive setup evaluates the OSR models’ ability to detect the full-label and super-label shifts. Note that in the multi-label setting, we have larger test sets and more complex mixture cases, which

Method	VOC-6/14		COCO-20/60	
	$\mathcal{H}$ AUROC $\uparrow$ / FPR@95 $\downarrow$	$\mathcal{M}$ AUROC $\uparrow$ / FPR@95 $\downarrow$	$\mathcal{H}$ AUROC $\uparrow$ / FPR@95 $\downarrow$	$\mathcal{M}$ AUROC $\uparrow$ / FPR@95 $\downarrow$
CSSR [16]	70.1 / 95.8	53.8 / 96.2	68.7 / 91.9	56.1 / 97.0
MLS [37]	63.5 / 91.3	55.9 / 93.3	76.3 / 86.8	67.8 / 90.1
ARPL [2]	62.5 / 93.1	56.0 / 92.0	77.8 / 84.5	68.1 / 89.0
DIAS [29]	62.4 / 93.5	53.6 / 93.2	65.5 / 92.1	61.4 / 92.9
VIT-MLS	92.1 / 56.6	67.2 / 88.1	90.6 / 69.2	73.8 / 84.9
OpenSlot	<b>93.2 / 53.3</b>	<b>71.3 / 86.7</b>	<b>91.6 / 70.1</b>	<b>74.9 / 83.1</b>

TABLE I: **Single-label.** In this paper, we utilize  $\mathcal{H}$  and  $\mathcal{M}$  to refer to the UUC-only test set and the mixed test sets that contain both KKCs and UUCs. Our results, scored using the energy function [27], consistently outperform existing studies.

evaluate OSR models’ robustness. Detailed class splits and benchmark information are provided in the Appendix.

- **Conventional OSR:** We also evaluate OpenSlot on three conventional OSR benchmarks: CIFAR-6/4 [20], CIFAR-50/50, and TinyImageNet-(20/180) [22]. To ensure a fair comparison with existing studies, we adopt the official KKC/UUC splits from the OpenOOD [40] benchmark.

**Baselines & Metrics.** For single-label tasks of the mixed OSR, we compare OpenSlot with state-of-the-art (SOTA) methods. Since there are no specific OSR studies for the multi-label setting, we use ResNet50 [12] for classification training and score predictions with out-of-distribution (OOD) detection functions [13], [23], [38] to build baselines for comparison.

For the conventional OSR tasks, we follow protocols in [8], [40] and compare our OpenSlot with existing studies [29], [36]. We evaluate all results with two metrics: 1) the threshold-free area under the Receiver-Operator curve (AUROC), and 2) the false-positive rate at 95% true-positive rate (FPR@95).

**Implementation details.** In the pre-training on VOC and COCO, we follow the configurations in [33], setting the number of slots to 6 and 7, respectively. For experiments in conventional OSR benchmarks [40], we set the slot number to 5. After the classification training, we obtain 79.0/74.2 Acc in the closed sets of single-label VOC/COCO and 71.2/65.6 mAP in the multi-label cases, respectively.

### B. Results of OSR

This part reports the mixed OSR results on the constructed single & multi-label benchmarks. Additionally, we evaluate the performance of OpenSlot on conventional OSR datasets.

**Single-label.** Tab. I compares OpenSlot with existing OSR methods, including CSSR [16], ARPL [2], MLS [37], and a transformer baseline VIT-MLS. First, all baselines experience a substantial accuracy degradation on the mixed test set  $\mathcal{M}$  (compared to  $\mathcal{H}$ ). This indicates that the super-label shift in the mixed OSR is more challenging than the conventional full-label shift, revealing the existing models’ limitations in processing mixed semantics.

In contrast, OpenSlot outperforms all baselines across benchmarks. Specifically, on the  $\mathcal{M}$  sets of the two benchmarks, we obtain improvements of 4.1% and 1.1% in AUROC and reductions of 1.4% and 1.8% in FPR@95 compared to the best baseline results. This demonstrates that OpenSlot can better handle images with mixed class types and distinguish between known and unknown class objects.

**Multi-label.** Tab. II reports our comparison results with different OOD detection methods (working with ResNet50). For a

Method	VOC-COCO (20/60)		COCO					
	$\mathcal{H}$	$\mathcal{M}$	Task1 (20/60)		Task2 (40/40)		Task3 (60/20)	
	AUROC $\uparrow$ / FPR@95 $\downarrow$	AUROC $\uparrow$ / FPR@95 $\downarrow$	$\mathcal{H}$	$\mathcal{M}$	$\mathcal{H}$	$\mathcal{M}$	$\mathcal{H}$	$\mathcal{M}$
Mahalanobis [23]	80.3 / 56.7	61.2 / 87.8	82.3 / 70.3	74.0 / 70.3	72.5 / 79.2	63.3 / 92.3	74.0 / 78.1	64.1 / 91.5
MaxLogit [37]	53.5 / 96.0	37.0 / 99.6	39.3 / 98.9	28.4 / 99.2	41.4 / 94.8	39.2 / 96.9	49.2 / 96.6	32.2 / 98.7
Odin [24]	67.3 / 59.8	42.7 / 92.7	69.4 / 59.1	44.4 / 93.3	74.8 / 53.3	38.6 / 93.2	83.3 / 50.1	40.7 / 93.3
JointEnergy [38]	85.9 / 58.6	47.9 / 91.8	92.0 / 48.1	57.7 / 89.7	91.0 / 53.4	58.1 / 92.0	92.7 / 46.0	58.4 / 90.9
OpenSlot (ResNet34)	84.7 / 64.8	71.5 / 85.3	82.7 / 75.4	75.9 / 81.5	84.1 / 69.2	64.2 / 91.4	83.9 / 72.6	69.3 / 90.8
OpenSlot (ViT-B16)	84.4 / 65.0	<b>70.0 / 84.3</b>	84.8 / 74.7	<b>78.0 / 82.3</b>	83.7 / 69.1	<b>67.5 / 90.6</b>	84.5 / 69.5	<b>70.3 / 89.1</b>

TABLE II: **Multi-label OSR.** Values in brackets are the number of KKC/UUCs. Bold and underlined indicate the best and the second-best results by ours (with the energy [27]). We test OpenSlot using ResNet34 [12] and ViT-B16 [6] as the encoder for training and report their OSR results, respectively.

Method	CIFAR-6/4	CIFAR-50/50	Tiny-20/180
ODIN [24]	72.1	80.3	75.7
MSP [13]	85.3	81.0	73.0
MLS [37]	84.8	82.7	75.5
KNN [36]	86.9	83.4	74.1
OpenSlot	<b>87.4</b>	<b>83.7</b>	<b>78.5</b>

TABLE III: Results (AUROC  $\uparrow$ ) of **conventional OSR.** The reported baseline results are from [40]. OpenSlot achieves SOTA results on these conventional benchmarks [20], [22].

fair comparison, we also train OpenSlot with the ResNet34 encoder and MLP decoder design [33] and conduct OSR evaluation. On the  $\mathcal{H}$  (full-label shift) test set, OpenSlot falls behind the leading baseline, JointEnergy [38], though it remains competitive with others.

The comparison on the  $\mathcal{M}$  set reveals that the ViT encoder exhibits a slight performance advantage over ResNet34, and OpenSlot significantly exceeds the baselines regardless of the encoder choice. These observations suggest that our model is robust in handling mixed scenarios, demonstrating strong potential in real-world applications, e.g., detecting unknown obstacles in robotic environments or identifying unseen lesions or abnormalities within the same medical image.

**Conventional OSR.** We report the comparison results in Tab. III. On the homogeneous unknown test set  $\mathcal{H}$  (indicating the full-label shift), our method outperforms all baselines across three benchmarks, achieving state-of-the-art performances on these conventional datasets. This remarkable performance demonstrates the advantages of our proposed approach in detecting the full-label shift against conventional OSR methods.

### C. Ablation studies

This section tests the feasibility of OpenSlot. First, we display the semantic misalignment problem during slot predictions and discuss the effect of our ANS. Finally, we ablate the scoring functions, aggregation schemes, and hyperparameters. **The Semantic misalignment problem.** Using object-centric learning, we represent image semantics with a fixed set of slot features, each producing a class prediction. However, noise (background & invalid) slots exist in every image and are likely to be incorrectly matched with the true class labels during Hungarian matching. We observe that the slots contributing to class predictions tend to represent noise rather than class objects. We call this misalignment between predictive slots and true class semantics ‘‘semantic misalignment’’.

To show the threat of this problem, we consider the single-label classification task as an example; its class prediction is

determined by the max-logit slot, the slot with the highest logit from the main classifier  $\varphi_{fg}$ . We utilize the ground-truth (GT) segmentation masks to label the object semantics captured by each slot. Specifically, we compute the valid semantic region for all slots (using attention masks) and select the one with maximum overlap with GT as the foreground (FG) slot, i.e., the true class object; while the remaining slots are labeled as Noise. In Fig. 4 (left), we display the distribution of the max-logit slot across the FG and Noise groups. The right side of Fig. 4 shows the average logit norms of these two groups.

When employing the naive approach (Pure Slot, described in Section IV), we observe that the max-logit slot is prone to falling into the Noise group. Besides, by sorting the slots in ascending order based on their logit values from  $\varphi_{fg}$  and visualizing their attention masks in Fig. 5, we note that the noise slots have larger logit values than the FG slots, consistent with the distribution shown in Fig. 4.

These observations indicate the Pure Slot method (without ANS) can be easily confused by noise slot features in the classification training, failing to capture the true class semantics. **Effects of ANS.** By comparison (Fig. 4, ours), ANS ensures that the max-logit slot falls into the FG group, aligning with the true class semantics. Furthermore, ANS increases the logit value gap between the FG and Noise slot groups.

Meanwhile, we perform a similar sorting and visualization analysis of the attention masks in Fig. 6. On the right side, the main classifier  $\varphi_{fg}$  suppresses noise and assigns the slot representing the true class object with the largest logit value. This finding is consistent with Fig. 4 (ours). On the left figure, the sorted slots based on the outputs from the noise classifier  $\varphi_{nz}$  showcase that  $\varphi_{nz}$  accurately discriminates noise features.

Fig. 4 and the comparison between Fig. 5 and 6 showcase that our ANS method effectively separates the noise slots and excludes them from the class classification. During inference, when computing OSR scores for positive and negative images, the noise slots of both images would output similar values. This ensures that the primary score value gap between the positive and the negative stems from the semantic difference of class objects, leading to a clear class decision boundary.

Finally, we quantitatively compare Pure Slot and our OpenSlot in Tab. IV. Our consistent performance gains achieved on both the  $\mathcal{M}$  and  $\mathcal{H}$  test sets across two benchmarks verify the benefits of ANS in enhancing the capability of slots to detect both super-label and full-label shifts.

**Choice of scoring functions.** To obtain the OSR results, we score the slot-based class predictions. We evaluate various out-

Method	VOC-6/14		COCO-20/60	
	$\mathcal{H}$	$\mathcal{M}$	$\mathcal{H}$	$\mathcal{M}$
Pure Slot	80.4 / 76.7	55.7 / 92.1	76.0 / 78.8	67.8 / 84.7
Ours	92.0 / 56.3	67.3 / 88.4	86.7 / 62.7	73.5 / 79.7

TABLE IV: Anti-noise-slot (ANS) evaluation. All results are AUROC  $\uparrow$  / FPR@95  $\downarrow$ .

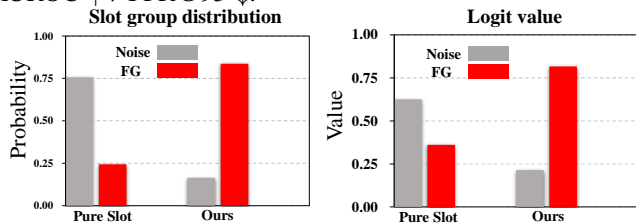


Fig. 4: To compare OpenSlot with the Pure Slot baseline, we divide all slots into the foreground (FG) and Noise groups based on the semantics denoted by each slot. We then show the distribution of the max-logit slot (with the highest logit value from  $\varphi_{fg}$ ) across these two groups (**Left**). Besides, we present each group’s logit norm (**right**) (after Min-max normalization).

of-distribution (OOD) detection methods, including four logit-based: MSP [13], ODIN [24], Energy [27], MaxLogit [37], as well as the feature-based Mahalanobis distance [23]. In Tab. V, we compare their performances. When combined with OpenSlot, MaxLogit and Energy [27] consistently outperform other scoring methods, yielding superior OSR results.

**Effects of score aggregation methods.** This part investigates the impact of score aggregation schemes on OSR results. We combine the scores from all (All) slots to represent the test sample’s overall “knownness” level. Besides, we design a selective (Sel.) scheme as an alternative. Specifically, we utilize the noise classifier  $\varphi_{nz}$ ’s predictions to identify the foreground (FG) slots (with scores below a threshold  $\gamma$ ) and the noise slots. During inference, we only aggregate the scores of the determined FG slots. Scoring with the energy method [27], we report the size of the FG group (as a percentage of the entire slot set) when using different  $\gamma$  values, and their OSR results.

In Tab. VI, we observe a minor performance (AUROC) gap (when  $\gamma = 0.75$ ) between two schemes on the mixed  $\mathcal{M}$  set. Notably, the determined FG group comprises only around 30% of the slot set. This observation suggests that the basis for OpenSlot’s OSR decision stems from the detected semantic differences among the class objects, i.e., unknown unknown classes (UUCs), in the FG group rather than from noise slots. This finding further verifies ANS’s effect on noise separation.

**Effects of hyperparameters.** Here we ablate two hyperparameters: the attention threshold  $\alpha$  and noise threshold  $\beta$ .

Tab. VII reports the OSR results when setting  $\alpha$  and  $\beta$  of different values. We observe that OpenSlot reaches the best performances when  $\alpha = 0.50$  and  $\beta = 0.75$  on both benchmarks. Besides, these ablation results suggest that  $\beta$  has a larger effect on OSR results than  $\alpha$ , showing the importance of noise discrimination in slot predictions.

#### D. Effect of slot prediction in OSR scoring

In this section, we compare OpenSlot with conventional OSR models to test the effectiveness of slot-based predictions in addressing the mixed OSR problem. We do this by analyzing the differences in their respective scoring mechanisms.

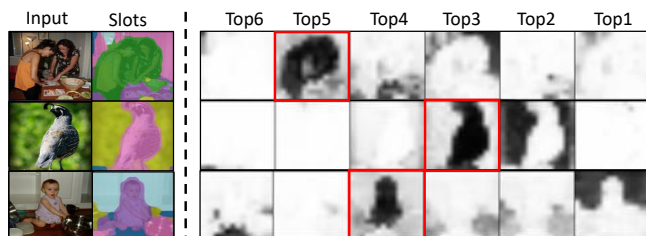


Fig. 5: Display of the semantic misalignment problem. After pre-training, we learn slots for semantic representation (in different colors). In Pure Slot, we train the main classifier  $\varphi_{fg}$  with vanilla Hungarian matching. When sorting (ascending) all slots by  $\varphi_{fg}$ ’s output and displaying their attention masks (Top 6  $\rightarrow$  Top 1), we find that the noise (invalid & background) slots have larger logit values than the true class slots (marked with red), indicating that  $\varphi_{fg}$  is confused by noise slots.

OOD Metrics	VOC-6/14		COCO-20/60	
	$\mathcal{H}$	$\mathcal{M}$	$\mathcal{H}$	$\mathcal{M}$
Mahalanobis [23]	82.7 / 81.7	50.1 / 95.2	87.0 / 79.4	50.7 / 97.7
MaxLogit [37]	92.0 / 56.3	67.3 / 89.2	88.4 / <b>62.7</b>	73.5 / <b>79.7</b>
MSP [13]	89.1 / 69.1	64.6 / 90.2	80.7 / 79.9	69.4 / 85.3
Odin [24]	92.0 / <b>51.5</b>	66.4 / 88.5	84.2 / 73.0	69.7 / 83.2
Energy [24]	<b>93.2</b> / 53.3	<b>71.3</b> / <b>86.7</b>	<b>89.6</b> / 70.1	<b>74.9</b> / 83.1

TABLE V: Ablation results (AUROC  $\uparrow$  / FPR@95  $\downarrow$ ) of OpenSlot using different OOD detection functions. The Energy [27] and Maxlogit [37] are better metrics for OpenSlot.

Given an input image  $I \in \mathbb{R}^{H \times W \times 3}$  with multiple class semantics, a conventional OSR approach (either with the CNN/ViT) is to use classifier  $f$  maps the semantic features of  $I$  to  $\hat{l} \in \mathbb{R}^{|\mathcal{K}|}$  and get  $|\mathcal{K}|$  (the number of KKC) logit values. Based on  $\hat{l}$ , we compute a deterministic score for OSR evaluation. By contrast, our method uses the classifier  $f_{slot}$  across slots and gets  $\hat{l}_{slot} \in \mathbb{R}^{N \times |\mathcal{K}|}$ , where each slot has an independent class prediction for the denoted object semantic.

Fig. 7 presents an example comparison between JointEnergy [38] and our OpenSlot, when feeding a positive and a mixed negative image. JointEnergy [38] displays nearly no difference in the scores between the two samples (64.6 vs. 64.0). It is because its  $\hat{y}$  is built upon the global semantic content of the image  $I$ , which is largely affected by the

Scheme	$\gamma$	FG (%)	$\mathcal{H}$		$\mathcal{M}$	
			$\mathcal{H}$	$\mathcal{M}$	$\mathcal{H}$	$\mathcal{M}$
Sel.	0.05	9.2	68.7 / 86.7	57.4 / 90.4		
	0.25	25.9	84.2 / 74.1	64.6 / 88.1		
	0.50	27.0	86.3 / 73.8	65.6 / 87.6		
	0.75	32.1	89.1 / 77.2	67.0 / 89.6		
All	-	-	93.2 / 53.3	71.3 / 86.7		

TABLE VI: Effects of  $\gamma$ . We test on the single-label VOC and use [27] for OSR evaluation (AUROC  $\uparrow$  / FPR@95  $\downarrow$ )

$\alpha$	$\beta$	VOC-6/14		COCO-20/60	
		$\mathcal{H}$	$\mathcal{M}$	$\mathcal{H}$	$\mathcal{M}$
0.25	0.25	71.1 / 80.9	53.4 / 96.4	69.1 / 82.7	51.1 / 97.6
	0.50	84.3 / 70.5	59.7 / 93.6	77.8 / 75.4	61.7 / 90.1
	0.75	89.1 / 62.5	63.7 / 90.5	82.9 / 69.4	70.7 / 85.8
0.50	0.25	76.6 / 79.7	56.1 / 94.7	77.1 / 80.6	63.1 / 91.8
	0.50	82.7 / 75.4	59.1 / 92.3	78.4 / 74.5	64.7 / 87.8
	0.75	<b>92.0 / 56.3</b>	<b>67.3 / 88.4</b>	<b>86.7 / 62.7</b>	<b>73.5 / 79.7</b>
0.75	0.25	76.8 / 77.4	62.5 / 91.7	76.1 / 76.4	65.9 / 91.7
	0.50	84.9 / 70.8	62.9 / 90.4	80.2 / 70.3	69.8 / 87.5
	0.75	90.9 / 60.1	65.8 / 89.3	85.1 / 64.2	72.7 / 80.9

TABLE VII: Effects (AUROC  $\uparrow$  / FPR@95  $\downarrow$ ) of the attention threshold  $\alpha$  and the noise threshold  $\beta$ . We get the best results when setting  $\alpha$  and  $\beta$  to 0.50 and 0.75, respectively.

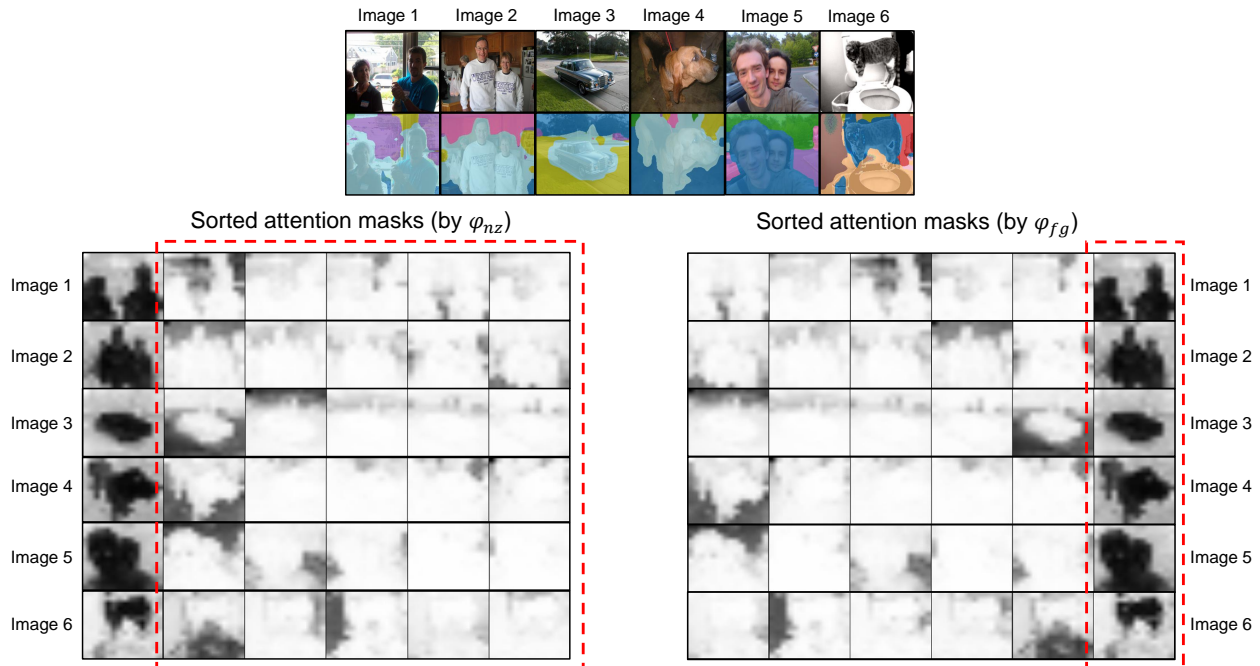


Fig. 6: Demonstration of ANS’ effects on slot separation. Our ANS excludes noise slots from Hungarian matching and enlarges their logit gap against the true class slots during training. In this example, we sort (ascending) attention masks based on slots’ logit from the main classifier  $\varphi_{nz}$  and the noise classifier  $\varphi_{fg}$ , respectively. In the right figure, the true class slots (cropped part) get the largest logit values. Meanwhile,  $\varphi_{nz}$  (the left figure) can discriminate noise slots (cropped part).

prominent known classes. The label shift of the inconspicuous unknown class (“handbag”) is covered by high scores in known class channels (Fig. 7, bottom left), making the negative indistinguishable from the positive in terms of score values.

By contrast, our slot approach addresses the threat of known classes in the mixed OSR problem by producing independent class predictions for captured image semantics. During inference, every slot prediction in  $f_{slot}$  is measured with the score function and is counted for OSR evaluation, without effects from others. In (Fig. 7, bottom right), we observe that the score gap between the positive and the negative image primarily comes from the detected unknown class object.

**Limitations.** Although exceeding existing OSR studies in detecting the super-label shift, OpenSlot underperforms the best method when handling the full-label shift in the multi-label setting. We attribute this to our model’s inferior classification accuracy in the closed set, and consider that other matching/cost computation methods [42] could be potential solutions, which we leave for future investigation.

### E. Yielding Benefits to Open-Set Object Detection

Apart from providing a binary decision on known and unknown, OpenSlot can also localize unknown class objects within images to explicitly explain the label shift, thus achieving the effect of open-set object detection (OSOD).

Following the setup in [8], we choose VOC as the close-set data and test on open-set images from COCO and OpenImages [21]. During training, OpenSlot only uses class labels.

**Results.** Table VIII compares OpenSlot with existing OSOD studies. Without employing a Region Proposal Network [32], OpenSlot even outperforms several object detector-based approaches and achieves performance comparable to SIREN-

Method	COCO	OpenImages
MSP [13]	83.5 / 71.0	81.9 / 73.1
ODIN [24]	82.2 / 59.8	82.6 / 63.1
KNN [36]	87.1 / 52.7	84.5 / 53.7
Energy score [27]	83.7 / 56.9	83.0 / 58.7
VOS [8]	88.7 / 47.5	85.2 / 51.3
SIREN-vMF [7]	85.4 / 64.7	82.8 / 68.5
Ours	85.2 / 66.3	83.4 / 61.8

TABLE VIII: Open-set object detection results (AUROC  $\uparrow$  / FPR@95  $\downarrow$ ). Without using bounding boxes in training, our method outperforms several detector-based studies.

vMF [7]. Fig. 8 presents example results where our method corrects the mispredictions of the object detector, reducing the false positive rate.

Notably, unlike traditional methods that rely on predefined classes and selective search algorithms for proposal generation, OpenSlot discovers objects from image data in an unsupervised manner [1], [33], and can obtain robust object representations against domain shifts [5]. When tested on open-set images with significant domain differences from the closet-set (Fig. 9), these properties ensure that OpenSlot identifies different objects of interest, leading to improved localization of unknown objects. and reflecting our slot approach’s stronger generalization ability than detector-based methods.

**Overhead comparison.** Tab. IX compares the computational cost of OpenSlot and Faster R-CNN [32] from different perspectives. We have a lightweight and with only 2.4 million parameters (including the pre-train and the classification models), and require merely 3.5 hours for training. This cost is significantly lower than object detector models. Moreover, OpenSlot demonstrates faster inference time when generating object detection results, highlighting its efficiency advantages.

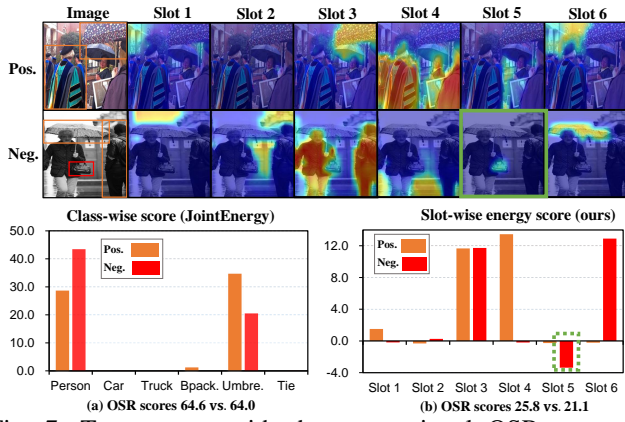


Fig. 7: To compare with the conventional OSR approach, we input the positive (Pos.) and the mixed negative (Neg.) samples into ResNet50 [38] and OpenSlot. (a) we compute JointEnergy [38] of two samples and show class-wise values. The positive and the negative image score 64.6 and 64.0, respectively. The known class objects (“Umbre.” and “Person”) in the negative image have high scores in corresponding class channels, making their overall score value almost identical to the positive image. By contrast (b), we aggregate the slot prediction score [27] and obtain 25.8 vs. 21.1 for two samples. Combined with attention masks, we show that the unknown slot (“handbag”, slot 5) gets the lowest score, which provides meaningful discrimination information for OSR decisions.

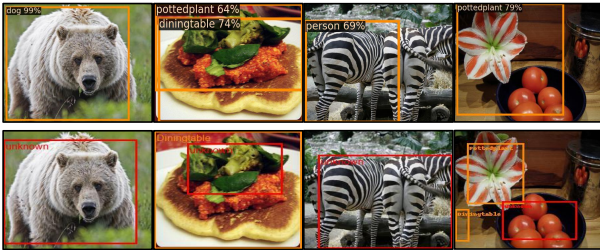


Fig. 8: Object detection results on open-set images by Faster-RCNN [32] (the top row) and ours (the bottom row). The close-set data is VOC. **Orange**: detected objects and classified as known **Red**: detected unknown objects. In this example, we correct the misprediction of Faster-RCNN and successfully localize unknown class objects.

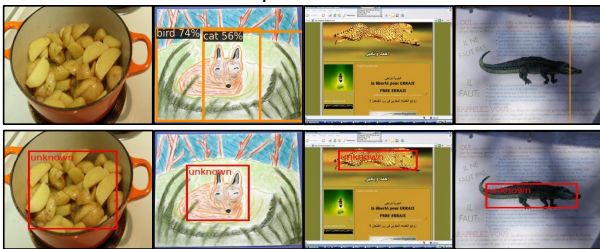


Fig. 9: Object detection results on open-set images with domain gap from the close-set data: Faster-RCNN (top) and ours (bottom). Faster-RCNN is constrained by the predefined classes in the close-set and fails to generate meaningful object proposals. By contrast, OpenSlot generates reliable objects of interest and distinguishes the known and unknown.

Method	Param.	Train. time	Infer. time
Faster-RCNN [32]	33.0 M	3.7 h	0.26 s
Ours	2.4 M	3.5 h	0.21 s

TABLE IX: We compare Faster-RCNN and OpenSlot on RTX3090, in terms of the parameter size (million, M), training time (hours, h), and inference speed (second/per image).

Tasks	$\mathcal{D}_{train}$	$\mathcal{D}_{test}^k$	$\mathcal{H}$	$\mathcal{M}$			
				$D$ -Easy	$D$ -Hard	$F$ -Easy	$F$ -Hard
VOC-6/14	2400	2709	641	709	380	1746	1361
COCO-20/60	8000	12892	61967	19625	1478	19320	13132
VOC-COCO	5717	10991	27135	33635	12063	21148	52335
Task1 (20/60)	9812	4877	31191	38348	8690	31966	43412
Task2 (40/40)	21235	10405	16868	17583	27411	19632	53063
Task3 (60/20)	46671	23124	7845	4131	29125	9430	34329

TABLE X: Summary of the single/multi-label OSR tasks. The values are the number of images in the individual datasets.

## VI. CONCLUSION

This paper introduced the mixed open-set recognition (OSR) problem, which considers the joint occurrence of unknown and known class objects in negative images. To tackle this challenge, we presented the OpenSlot framework, built upon the object-centric learning approach. Through the proposed anti-noise-slot (ANS) technique, we effectively excluded noisy slot features from the image classification process, addressing the semantic misalignment issue inherent in slot-based class predictions. Extensive experiments and ablation studies demonstrated OpenSlot’s superiority in handling the mixed OSR problem, significantly outperforming existing OSR studies and achieving SOTA results in conventional OSR benchmarks. Moreover, OpenSlot can be extended to open-set object detection to localize unknown class objects and explicitly explain label shifts. Competitive results and advantages in computational efficiency highlight the benefits of our model.

## APPENDIX

In this appendix, we introduce the detailed benchmark information and implementations.

### A. Mixed OSR

Pascal Voc (VOC) supports classification (VOC-Cls), segmentation (VOC-Seg). For the evaluation convenience, we use VOC-Seg in Tab. I and use the original COCO dataset.

**setup.** We merge each dataset’s training and validation set and perform the class split. First, we make a statistic about the object class distribution and find 6 VOC<sup>1</sup> and 20 COCO classes<sup>2</sup> have over 450 single-label images, which we consider as KKC candidates; the rest of the classes are used as UUCs.

For single-label tasks, we use all KKC and UUC candidates to construct VOC-6/14 and COCO-20/60. We use VOC-Cls and COCO to conduct the multi-label experiments and build up the test sets with the same criteria as the single-label setting. In COCO-20/60, 40/40, 60/20 tasks, KKC are randomly sampled, and the results vary with the sampling effects. We report the details of all OSR tasks in Tab. X:

### B. Experiment details

**Mixed OSR.** In single-label experiments, we set the learning rate (lr) as 0.0004 (half it every 40 epochs) and train the OpenSlot model for 200 epochs. We set lr to 0.005 and train 250 epochs in the multi-label case. Besides, we add a loss weight  $\lambda$  before the noise loss  $L_{nz}$  (Eq. 5) and set it to 0.01.

<sup>1</sup>“person”, “bird”, “car”, “cat”, “dog”, “person”

<sup>2</sup>“airplane”, “train”, “boat”, “traffic light”, “fire hydrant”, “stop sign”, “bench”, “bird”, “cat”, “horse”, “sheep”, “cow”, “elephant”, “bear”, “zebra”, “giraffe”, “toilet”, “clock”, “vase”, “ted. bear”

**Open-set object detection.** We use the noise classifier  $\varphi_{nz}$ 's predictions and a threshold (0.75) to determine the foreground (FG) slots (below threshold). We then mask (over 0.5) the pixels in the FG attention mask and consider the resulting binary mask as the slot's semantic region. Assuming a meaningful semantic object must be over 40 pixels, we obtain a valid object mask to compute bounding boxes. Finally, we score [27] all FG slots and consider those with scores over 5 as known objects and the rest as unknown.

## REFERENCES

- [1] M. Caron, H. Touvron, I. Misra, H. Jégou, J. Mairal, P. Bojanowski, and A. Joulin, "Emerging properties in self-supervised vision transformers," in *IEEE Conf. Comput. Vis. Patt. Recog.*, Seattle, USA, 2021, pp. 9650–9660.
- [2] G. Chen, P. Peng, X. Wang, and Y. Tian, "Adversarial reciprocal points learning for open set recognition," *IEEE Trans. Pattern Anal. Mach. Intell.*, vol. 44, no. 11, pp. 8065–8081, 2021.
- [3] Y. Cui, Z. Yu, W. Peng, Q. Tian, and L. Liu, "Rethinking few-shot class-incremental learning with open-set hypothesis in hyperbolic geometry," *IEEE Trans. on Multimedia*, pp. 1–14, 2023.
- [4] S. Deng, J.-G. Yu, Z. Wu, H. Gao, Y. Li, and Y. Yang, "Learning relative feature displacement for few-shot open-set recognition," *IEEE Trans. on Multimedia*, vol. 25, pp. 5763–5774, 2023.
- [5] A. Dittadi, S. Papa, M. De Vita, B. Schölkopf, O. Winther, and F. Locatello, "Generalization and robustness implications in object-centric learning," 2021. [Online]. Available: <https://arxiv.org/abs/2107.00637>
- [6] A. Dosovitskiy, L. Beyer, A. Kolesnikov, D. Weissenborn, X. Zhai, T. Unterthiner, M. Dehghani, M. Minderer, G. Heigold, S. Gelly *et al.*, "An image is worth 16x16 words: Transformers for image recognition at scale," 2020. [Online]. Available: <https://arxiv.org/abs/2010.11929>
- [7] X. Du, G. Gozum, Y. Ming, and Y. Li, "Siren: Shaping representations for detecting out-of-distribution objects," *Adv. Neural Inform. Process. Syst.*, vol. 35, pp. 20 434–20 449, 2022.
- [8] X. Du, Z. Wang, M. Cai, and Y. Li, "Vos: Learning what you don't know by virtual outlier synthesis," 2022. [Online]. Available: <https://arxiv.org/abs/2202.01197>
- [9] M. Everingham and J. Winn, "The pascal visual object classes challenge 2012 (voc2012) development kit," *Patt. Anal., Statist. Modelling and Computat. Learning, Tech. Rep.*, vol. 8, 2011.
- [10] C. Geng, S.-j. Huang, and S. Chen, "Recent advances in open set recognition: A survey," *IEEE Trans. Pattern Anal. Mach. Intell.*, vol. 43, no. 10, pp. 3614–3631, 2020.
- [11] X. Guo, J. Liu, T. Liu, and Y. Yuan, "Simt: Handling open-set noise for domain adaptive semantic segmentation," in *IEEE Conf. Comput. Vis. Patt. Recog.*, New Orleans, USA, 2022, pp. 7032–7041.
- [12] K. He, X. Zhang, S. Ren, and J. Sun, "Deep residual learning for image recognition," in *IEEE Conf. Comput. Vis. Patt. Recog.*, Las Vegas, USA, 2016, pp. 770–778.
- [13] D. Hendrycks and K. Gimpel, "A baseline for detecting misclassified and out-of-distribution examples in neural networks," 2016. [Online]. Available: <https://arxiv.org/abs/1610.02136>
- [14] C. Huang, Q. Xu, Y. Wang, Y. Wang, and Y. Zhang, "Mood 2020: A public benchmark for out-of-distribution detection and localization on medical images," *IEEE Trans. on Med. Imag.*, vol. 41, no. 10, pp. 2728–2738, 2022.
- [15] C. Huang and Q. e. a. Xu, "Self-supervised masking for unsupervised anomaly detection and localization," *IEEE Trans. on Multimedia*, vol. 25, pp. 4426–4438, 2023.
- [16] H. Huang, Y. Wang, Q. Hu, and M.-M. Cheng, "Class-specific semantic reconstruction for open set recognition," *IEEE Trans. Pattern Anal. Mach. Intell.*, vol. 45, no. 4, pp. 4214–4228, 2022.
- [17] J. Jiang, F. Deng, G. Singh, and S. Ahn, "Object-centric slot diffusion," 2023. [Online]. Available: <https://arxiv.org/abs/2303.10834>
- [18] J. Kim, J. Choi, H.-J. Choi, and S. J. Kim, "Shepherding slots to objects: Towards stable and robust object-centric learning," in *IEEE Conf. Comput. Vis. Patt. Recog.*, Vancouver, Canada, 2023, pp. 19 198–19 207.
- [19] S. Kong and D. Ramanan, "Opengan: Open-set recognition via open data generation," in *Int. Conf. Comput. Vis.*, Virtual/Online, 2021, pp. 813–822.
- [20] A. Krizhevsky, G. Hinton *et al.*, "Learning multiple layers of features from tiny images," 2009.
- [21] A. Kuznetsova, H. Rom, N. Alldrin, J. Uijlings, I. Krasin, J. Pont-Tuset, S. Kamali, S. Popov, M. Mallocci, A. Kolesnikov *et al.*, "The open images dataset v4: Unified image classification, object detection, and visual relationship detection at scale," *Int. J. Comput. Vis.*, vol. 128, no. 7, pp. 1956–1981, 2020.
- [22] Y. Le and X. Yang, "Tiny imagenet visual recognition challenge," *CS 231N*, vol. 7, no. 7, p. 3, 2015.
- [23] K. Lee, K. Lee, H. Lee, and J. Shin, "A simple unified framework for detecting out-of-distribution samples and adversarial attacks," *Adv. Neural Inform. Process. Syst.*, vol. 31, 2018.
- [24] S. Liang, Y. Li, and R. Srikant, "Enhancing the reliability of out-of-distribution image detection in neural networks," 2017. [Online]. Available: <https://arxiv.org/abs/1706.02690>
- [25] T.-Y. Lin, M. Maire, S. Belongie, J. Hays, P. Perona, D. Ramanan, P. Dollár, and C. L. Zitnick, "Microsoft coco: Common objects in context," in *Eur. Conf. Comput. Vis.* Zurich, Switzerland: Springer, 2014, pp. 740–755.
- [26] S. Liu, Z. Zeng, T. Ren, F. Li, H. Zhang, J. Yang, C. Li, J. Yang, H. Su, J. Zhu *et al.*, "Grounding dino: Marrying dino with grounded pre-training for open-set object detection," 2023. [Online]. Available: <https://arxiv.org/abs/arXiv:2303.05499>
- [27] W. Liu, X. Wang, J. Owens, and Y. Li, "Energy-based out-of-distribution detection," *Adv. Neural Inform. Process. Syst.*, vol. 33, pp. 21 464–21 475, 2020.
- [28] F. Locatello, D. Weissenborn, T. Unterthiner, A. Mahendran, G. Heigold, J. Uszkoreit, A. Dosovitskiy, and T. Kipf, "Object-centric learning with slot attention," *Adv. Neural Inform. Process. Syst.*, vol. 33, pp. 11 525–11 538, 2020.
- [29] W. Moon, J. Park, H. S. Seong, C.-H. Cho, and J.-P. Heo, "Difficulty-aware simulator for open set recognition," in *Eur. Conf. Comput. Vis.* Tel Aviv, Israel: Springer, 2022, pp. 365–381.
- [30] M. A. Munir, M. H. Khan, M. Sarfraz, and M. Ali, "Towards improving calibration in object detection under domain shift," *Adv. Neural Inform. Process. Syst.*, vol. 35, pp. 38 706–38 718, 2022.
- [31] S. Papa, O. Winther, and A. Dittadi, "Inductive biases for object-centric representations in the presence of complex textures," 2022. [Online]. Available: <https://arxiv.org/abs/2204.08479>
- [32] S. Ren, K. He, R. Girshick, and J. Sun, "Faster r-cnn: Towards real-time object detection with region proposal networks," *Adv. Neural Inform. Process. Syst.*, vol. 28, 2015.
- [33] M. Seitzer, M. Horn, A. Zadaianchuk, D. Zietlow, T. Xiao, C.-J. Simon-Gabriel, T. He, Z. Zhang, B. Schölkopf, T. Brox *et al.*, "Bridging the gap to real-world object-centric learning," 2022. [Online]. Available: <https://arxiv.org/abs/2209.14860>
- [34] G. Singh, F. Deng, and S. Ahn, "Illiterate dall-e learns to compose," 2019. [Online]. Available: <https://arxiv.org/abs/2110.11405>
- [35] G. Singh, Y.-F. Wu, and S. Ahn, "Simple unsupervised object-centric learning for complex and naturalistic videos," *Adv. Neural Inform. Process. Syst.*, vol. 35, pp. 18 181–18 196, 2022.
- [36] Y. Sun, Y. Ming, X. Zhu, and Y. Li, "Out-of-distribution detection with deep nearest neighbors," in *Int. Conf. on Mach. Learn.* Baltimore, USA: PMLR, 2022, pp. 20 827–20 840.
- [37] S. Vaze, K. Han, A. Vedaldi, and A. Zisserman, "Open-set recognition: A good closed-set classifier is all you need?" 2021. [Online]. Available: <https://arxiv.org/abs/2110.06207>
- [38] H. Wang, W. Liu, A. Bocchieri, and Y. Li, "Can multi-label classification networks know what they don't know?" *Adv. Neural Inform. Process. Syst.*, vol. 34, pp. 29 074–29 087, 2021.
- [39] J. Wu, J. Wang, Z. Yang, Z. Gan, Z. Liu, J. Yuan, and L. Wang, "Grit: A generative region-to-text transformer for object understanding," 2022. [Online]. Available: <https://arxiv.org/abs/2212.00280>
- [40] J. Yang, P. Wang, D. Zou, Z. Zhou, K. Ding, W. Peng, H. Wang, G. Chen, B. Li, Y. Sun *et al.*, "Openood: Benchmarking generalized out-of-distribution detection," *Adv. Neural Inform. Process. Syst.*, vol. 35, pp. 32 598–32 611, 2022.
- [41] J. Yang, K. Zhou, Y. Li, and Z. Liu, "Generalized out-of-distribution detection: A survey," 2021. [Online]. Available: <https://arxiv.org/abs/2110.11334>
- [42] Y. Zhang, J. Hare, and A. Prugel-Bennett, "Deep set prediction networks," *Adv. Neural Inform. Process. Syst.*, vol. 32, 2019.
- [43] Z. Zhao, J. Wang, M. Horn, Y. Ding, T. He, Z. Bai, D. Zietlow, C.-J. Simon-Gabriel, B. Shuai, Z. Tu *et al.*, "Object-centric multiple object tracking," in *Int. Conf. Comput. Vis.*, Paris, France, 2023, pp. 16 601–16 611.